ACS Sustainable Chemistry & Engineering

Research Article

pubs.acs.org/journal/ascecg

Low-Cost Y-Doped TiO_2 Nanosheets Film with Highly Reactive {001} Facets from CRT Waste and Enhanced Photocatalytic Removal of Cr(VI) and Methyl Orange

Qijun Zhang,*[,†] Yu Fu,[†] Yufeng Wu,*[,†] Yi-Nan Zhang,[‡] and Tieyong Zuo[†]

[†]Institute of Circular Economy, Beijing University of Technology, Beijing 100124, People's Republic of China

[‡]Institute of Biomaterials and Biomedical Engineering, University of Toronto, Toronto, Ontario M5S 3G9, Canada

Supporting Information

ABSTRACT: In this paper, efficiency recovery of rare earth elements from cathode ray tubes (CRT) waste. Moreover, recycled yttrium was also served as raw material to produce a low-cost Y-doped TiO_2 nanosheets film with exposed {001} facets. An etching/dissolution growth mechanism was postulated by systematically investigating the influence of the reaction time. The synergistic effect of the Y dopant and the dominant {001} facets endows TiO_2 nanosheets film with excellent activity in the photoremoval of Methyl Orange (MO) and Cr(VI). A possible mechanism of photoremoval of MO and Cr(VI) is proposed. This study not only contributes to recycling methods for CRT waste but also presents a new way to prepare low-cost sustainable photocatalytic materials using economically viable waste.

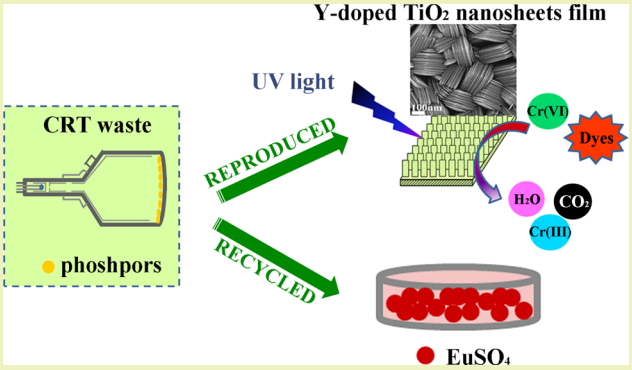

KEYWORDS: *CRT waste, Recycling, Rare earth elements, Y-doped, TiO_2 nanosheets, {001} facets, Photocatalytic activities*

INTRODUCTION

Nanophase anatase titanium dioxide (TiO_2), as the most promising semiconductor photocatalyst for a variety of solar-driven clean energy and environmental pollution treatment technologies, has been widely studied owing to its low cost, resistance to photocorrosion, biological and chemical inertness, and strong oxidizing properties.[1−3] However, practical applications of TiO_2 nanoparticles as a photocatalyst are greatly restricted by the low quantum yield caused by the high electron−hole pair recombination rate and the difficulty of separating the suspended nanoparticles from aqueous solutions for reuse.[4−6] To solve these problems, many recent works have attempted to immobilize TiO_2 on a solid carrier and/or change the electronic structure of the TiO_2 via doping with metallic and nonmetallic elements.[4,7−9] Recently, doping with rare-earth elements (REEs) has shown great potential,[10,11] because: (1) REEs has a 4f electron configuration, which reduces electron−hole pair recombination; and (2) REEs doping can promote the chemical adsorption of organic substrates on the TiO_2 crystal surfaces and improve its photocatalytic efficiency. However, using REEs-doped TiO_2 photocatalysis materials in practical applications it is a challenge because the prices for these metals have been generally increasing over the past few years.

Cathode ray tubes (CRT), which contain a considerable amount of rare earth, are a significant component of display devices such as computer monitors and TVs. With the development of the information technology and electronic industry, display devices with CRTs have been replaced by new products such as liquid crystal displays (LCDs) and plasma display panels (PDPs).[12,13] As a result, enormous amounts of CRT waste are constantly generated every year worldwide. Generally, an ordinary CRT display unit is composed of approximately 63.2 wt % of screen glass, 24.0 wt % of cone glass, 0.4 wt % of a getter plus an electron gun, 0.4 wt % of ceramic seal and 0.04 wt % of phosphor powders.[14] Although the glass, metal and ceramic materials in the CRT are often recycled, the phosphor powders are usually simply discarded or stockpiled, despite their high content of valuable REEs, such as yttrium and europium.[15,16] Recovering REEs from CRT phosphor waste is, therefore, interesting and important in terms of both waste treatment and the recovery of economically viable raw materials for low-cost synthesis of photocatalysis materials.

It has been demonstrated that TiO_2 catalytic properties, especially its photocatalytic activities, are closely associated with its exposed facets.[17] Therefore, increasing research attention is now being directly toward engineering the surface structure of TiO_2 at the most fundamental and atomic level, namely the morphological control of the {001} facets in the microscale and nanoscale range to fine-tune its photocatalytic activities.[18−21]

Received: December 28, 2015
Revised: January 18, 2016
Published: January 26, 2016

ACS Publications © 2016 American Chemical Society

DOI: 10.1021/acssuschemeng.5b01783
ACS Sustainable Chem. Eng. 2016, 4, 1794−1803

Scheme 1. Illustration of Recycling and Effective Synthesis Procedure of Low-Cost Y-Doped TiO_2 Nanosheets Film with Exposed {001} Facets from CRT Waste[a]

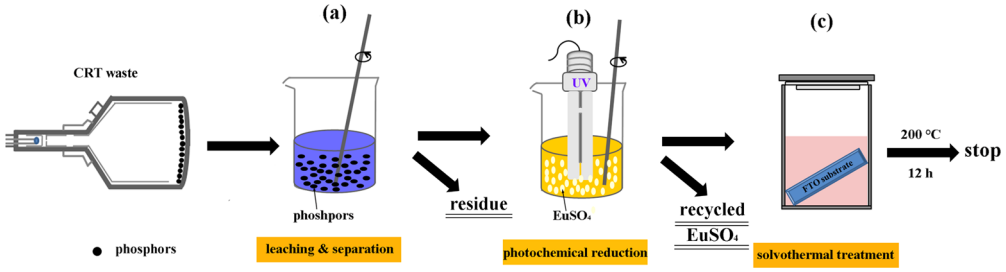

[a](a) Leaching and separation of REEs, (b) recycling of Y and Eu, and (c) synthesis of Y-doped TiO_2 nanosheets film.

For example, Han et al. synthesized anatase TiO_2 nanosheets with 89% of {001} facets via the hydrothermal reaction of tetrabutyl titanate and hydrofluoric acid.[19] The as-synthesized anatase TiO_2 nanosheets exhibited superior photocatalytic efficiencies, which exceeded that of commercial P25 TiO_2. This finding implies that both morphologically controlling anatase TiO_2 to expose the {001} facets and doping with REEs will obtain enhanced photocatalytic activities.

This work focuses on recovering yttrium and europium from CRT phosphor waste and using recycled yttrium as a dopant to produce Y-doped TiO_2 nanosheets film with exposed highly reactive {001} facets. The chemical, mineralogical and morphological characteristics of the phosphor waste, recycled components and the as-synthesized Y-doped TiO_2 nanosheets film were studied. The corresponding photocatalytic activities of the resultant Y-doped TiO_2 nanosheets film were evaluated for the photocatalytic reduction of Cr(VI) and the photodegradation of Methyl Orange (MO) aqueous solutions under UV light irradiation. Moreover, to the best of our knowledge, there are no reports investigating the use of CRT phosphor waste for the preparation of Y-doped TiO_2 nanosheets film with dominant {001} facets.

EXPERIMENTAL SECTION

Chemicals and Materials. The CRT waste was supplied by Shenzhen Green Eco-manufacture Hi-tech Co., Ltd.. The as-received CRT waste was crushing, grinding and dried at 110 °C until a constant weight was achieved. To homogenize the particle size and remove larger impurities such as glass particles and light films with high aluminum contents, the samples were milled using a planetary mill (72 h, 400 rpm) and passed through a 0.074 mm sieve before use. The rest of the reagents were all analytical grade and were purchased from the Chemical Reagent Company of Beijing.

Proposed Process. The proposed procedure of the anatase Y-doped TiO_2 nanosheets film with exposed {001} facets from CRT waste is divided into the following stages: (a) leaching and separation of REEs, (b) recycling of Y and Eu, and (c) synthesis of Y-doped TiO_2 nanosheets film, as shown in Scheme 1.

Leaching and Separation of REEs. A traditional wet metallurgy procedure was used to leach and separate REEs from CRT phosphor waste. First, 50 g of CRT phosphor waste samples was leached with 1 L, 3 M sulfuric acid and 5 mL of H_2O_2 at 50 °C for 2 h with stirring (300 rpm). Then, the resulting solutions were filtered to produce Y−Eu sulfate solutions. Finally, the Y−Eu sulfate solutions were separated and purified by traditional ammonia precipitation, oxalate precipitation and calcination, and Y_2O_3/Eu_2O_3 mixtures were obtained.

Recycling of Y and Eu. Recycling of Y and Eu from the as-obtained Y_2O_3/Eu_2O_3 mixtures followed a procedure from the literature with some modifications.[22] In a typical process, 5 g of as-obtained Y_2O_3/Eu_2O_3 mixtures were dissolved in 20 mL of hydrochloric acid (37%), and 50 mM $(NH_4)_2SO_4$ was added to achieve a sulfate:europium molar ratio of 7:1. Next, the pH was altered to 3.9 by adding drops of ammonia, 20 vol % of an isopropyl alcohol scavenger was added, and the solution was illuminated with 25 W UV Lamp for 72 h. After the photochemical treatment, the solutions were filtered, and Y-containing solutions and $EuSO_4$ were both obtained. Subsequently, the Y-containing solutions were slowly evaporated at 70−80 °C to obtain yttrium sulfate. The as-obtained yttrium sulfate can be used as a raw material to synthesize the Y-doped TiO_2 photocatalysis material.

Synthesis of Y-Doped TiO_2 Nanosheets Film. Y-doped TiO_2 nanosheets film with exposed {001} facets was fabricated by a solvothermal method. In a typical process, 10 mL of tetrabutyl titanate ($Ti(OBu)_4$) was added dropwise into acetic acid (40 mL) and the mixture was ultrasonicated for 15 min (500 W power). Then, appropriate amounts of the recovered Y-containing compounds were added to the above solution (Y/Ti = 0.75 mol %) and ultrasonicated for another 15 min. The mixed solution and 2 mL of HF (40%) were transferred to a stainless steel autoclave lined with polytetrafluoroethylene (Teflon) (100 mL). Next, an FTO substrate (F:SnO_2, TEC 15, Shenzhen CSG Float Glass Co. Ltd.), which had been ultrasonically cleaned for 60 min in a mixed solution of deionized water, acetone, and 2-propanol with a volume ratio of 1:1:1, was leaned at an angle against the wall of the Teflon liner with the conducting side facing down. The solvothermal synthesis was conducted at 200 °C for 12 h in an electric oven. After the synthesis, the autoclave was then removed from the oven and left to cool naturally to room temperature. The FTO substrate was removed, rinsed extensively with deionized water and ethanol, and fully dried at 60 °C in an oven. Subsequently, the films were heated to 600 °C at a heating rate of 1 °C min^{-1} and calcinated for 2 h to obtain a highly crystalline anatase phase.

Characterizations. The chemical composition of each solid sample was determined by X-ray fluorescence analysis (XRF) with a Philips PW2403 X-ray spectrometer (Philips, Holland). The concentrations of Y and Eu in each solution were analyzed by inductively coupled plasma-molic emission spectrometry (ICP-OES) with PerkinElmer's Optima 8000 (PerkinElmer, America). The crystal structure was examined by X-ray diffraction (XRD) analysis with a Bruker axs D8 Advance using Cu Kα radiation (Bruker, Germany). The morphology of the samples was examined by SU-8020 field-emission scanning electron microscopy (SEM) (Hitachi, Japan) and JEM-2100F high-resolution transmission electron microscopy (TEM) (JEOL, Japan). X-ray photoelectron spectroscopy (XPS) data were obtained with an ESCALab220i-XL electron spectrometer from VG Scientific using 300WAl KR radiation (E = 1486.6 eV) in a base pressure of 3×10^{-9} mbar. The binding energies were referenced to the C 1s line at 284.8 eV from adventitious carbon. The photoluminescence (PL) spectra were tested with a Japan Shimadzu RF-5301PC fluorescence spectrophotometer using a 355 nm line from a xenon lamp. The diffuse reflectance spectra (DRS) were characterized by an UV−vis spectrophotometer (UV 2550, Shimadzu, Japan).

Evaluation of Photocatalytic Activities. The evaluation of photocatalytic activity of the samples for the photocatalytic removal of Cr(VI) and MO in aqueous solutions was performed at ambient

DOI: 10.1021/acssuschemeng.5b01783
ACS Sustainable Chem. Eng. 2016, 4, 1794−1803

Table 1. Chemical Compositions (wt %) of CRT Phosphor Waste, The Leaching Residue, and the Recycled Y_2O_3/Eu_2O_3 Mixtures[a]

	Y_2O_3	Eu_2O_3	SO_3	ZnO	Al_2O_3	SiO_2	Fe_2O_3	PbO	BaO	K_2O
phosphor waste	16.79	1.07	39.37	33.42	6.43	1.86	0.36	0.32	0.20	0.18
leaching residue	0.75	N.D.[b]	47.94	45.74	0.67	3.59	0.38	0.51	0.42	N.D.
recycled Y_2O_3/Eu_2O_3	94.46	5.28	N.D.	0.02	0.06	0.06	0.07	0.05	N.D.	N.D.

[a]XRF analysis. [b]N.D.: not detectable.

temperature. $K_2Cr_2O_7$ was used as the sources of Cr(VI). In the photocatalytic experiment, all the as-prepared films of 2.0 cm × 4.0 cm were used. Prior to the photocatalytic activity measurements, the as-prepared samples were cleaned with 0.1 M NaOH aqueous solution and rinsed extensively with deionized water, and then dried at 60 °C. A 30 W UV lamp with a maximum emission at about 365 nm was used as the illumination source. For comparison purpose, the photocatalytic oxidation of MO and reduction of Cr(VI) by P25 TiO_2 films were also conducted. P25 TiO_2 films were prepared by screen printing of P25 TiO_2 paste on the FTO substrate (2.0 cm × 4.0 cm).[23] The as-prepared P25 TiO_2 film was sintered at 500 °C for 30 min.

For the photodegradation of aqueous MO, the films were immersed in 20 mL of the aqueous MO solution (10 mg/L) in a quartz cell. Prior to irradiation, all the films were dipped in a 20 mg/L MO solution for the saturated adsorption process. After irradiation for a given time, the concentration of MO in the resulting solution was analyzed by a Hitachi U-3900H spectrophotometer. The Lambert–Beer rule was applied using the characteristic absorbance band of the dye, 464 nm, to determine changes in concentration.

To evaluate the removal of Cr(VI) ions by photocatalyzed reduction, 20 mL of Cr(VI) solution with an initial concentration of 10 mg/L was circulated through a quartz tube. The pH value of the reaction suspension was adjusted to 2 using H_2SO_4 or NaOH. Before irradiation, the samples were placed in the dark to establish adsorption/desorption equilibrium. After various irradiation intervals, 0.1 mL volumes of the solution were taken from the reaction vessel for analysis. A spectrophotometer (Hitachi, U-3900H) was used to record the UV–vis absorption spectra of the solutions. Changes in the Cr(VI) concentration were followed by the spectrophotometric method of the diphenylcarbazide at 540 nm. All photocatalytic measurements were repeated twice to ensure the reliability of the results.

The photocatalytic stability of the Y-doped TiO_2 nanosheets film was also tested. After the photocatalytic reactions, the catalyst films were soaked in 10% HNO_3 solution for 12 h, subsequently washed with deionized water and ethanol several times and dried at 60 °C. After cleaning, the used Y-doped TiO_2 nanosheets films were tested in fresh solutions of MO and Cr(VI) under the sample experimental conditions as described above.

RESULTS AND DISCUSSION

Waste Characterizations and Recycling. The chemical compositions of CRT phosphor waste were analyzed by XRF. A large number of waste samples were studied, of which the common feature was a uniform composition. The phosphor waste is composed of SO_3 (39.37 wt %), ZnO (33.42 wt %), Y_2O_3 (16.79 wt %), Al_2O_3 (6.43 wt %), SiO_2 (1.86 wt %), and Eu_2O_3 (1.07 wt %) as the main components (Table 1). The chemical analysis is in agreement with the XRD pattern recorded for CRT phosphor waste (Figure 1a). As shown in Figure 1a, the main crystalline phases in the waste samples are $Y_2O_2S:Eu^{3+}$ (JCPDS No. 24-1424), ZnS (JCPDS No. 77-2100), $Ca_3Al_2P_2Si_2O_{15}$ (JCPDS No. 36-0108), and Al metal (JCPDS No. 85-1327). Figure S1 is a typical SEM image of CRT phosphor waste. It shows that CRT phosphor waste is a granular material composed of pseudopolyhedral particles with diameters ranging from 0.1 to 2.0 μm (Figure S1).

To evaluate the leaching of yttrium and europium, 50 g of CRT phosphor waste samples was leached with 1 L of sulfuric acid (3 mol/L) and 5 mL of H_2O_2 for 2 h with stirring (300 rpm) at 50 °C. The leaching residue was also analyzed by XRF, as shown in Table 1, which confirmed that the yttrium and europium contents totally dissolved in the acid solution. Figure 1b shows the XRD patterns of the leaching residue. The diffraction peaks agree with those of ZnS (JCPDS No. 77-2100) and S_8 (JCPDS No. 83-2285), whereas the $Y_2O_2S:Eu^{3+}$ peaks disappeared, confirming that yttrium and europium were completely leached out under these conditions. After leaching and filtering, the Y–Eu sulfate concentrate was obtained.

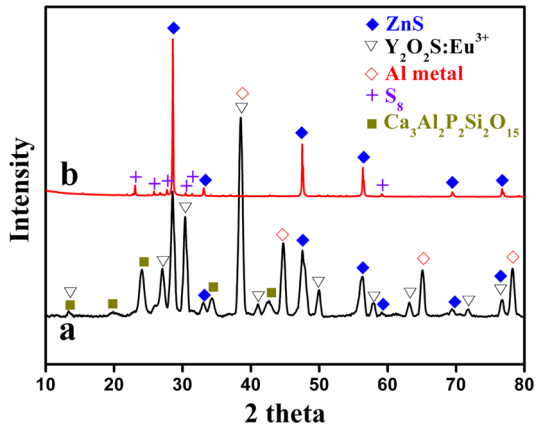

Figure 1. XRD patterns of (a) CRT phosphor waste and (b) the leaching residue.

After the separation and purification of Y–Eu sulfate solutions by traditional ammonia precipitation, oxalate precipitation and calcination, a product of 99.74% pure Y_2O_3/Eu_2O_3 mixtures was obtained, as shown in Figure 2a and Table 1. Next, the as-obtained Y_2O_3/Eu_2O_3 mixtures were treated using a photochemical reduction method (Figure S2). After 72 h of UV light irradiation, 99% of the europium was recycled as $EuSO_4$ with a purity of 97% (Figure 2b and Table S1). Finally, the yttrium-containing solutions were slowly evaporated at 70–80 °C to obtain yttrium sulfate. The as-obtained yttrium sulfate was used as a raw material to synthesize a Y-doped TiO_2 photocatalysis material.

Samples Preparation and Characterizations. *Morphologies and Structures.* The other aim of this work was to synthesize low-cost Y-doped TiO_2 nanosheets film on FTO substrate using recycled yttrium sulfate as a dopant source. We therefore performed a solvothermal treatment with $Ti(OBu)_4$ in acetic acid, which was combined with the recycled yttrium sulfate and hydrofluoric acid mixture, and the cleaned FTO substrate was placed into the reaction mixture. The morphology and structure of the as-obtained Y-doped TiO_2 nanosheets film were characterized by SEM and TEM as shown in Figure 3. A top view of the Y-doped TiO_2 nanosheets film in Figure 3a reveals that numerous irregular-shaped nanosheets are uniformly and densely distributed on the FTO substrate with an average lateral size of 1.5 μm. Higher magnification of

DOI: 10.1021/acssuschemeng.5b01783
ACS Sustainable Chem. Eng. 2016, 4, 1794–1803

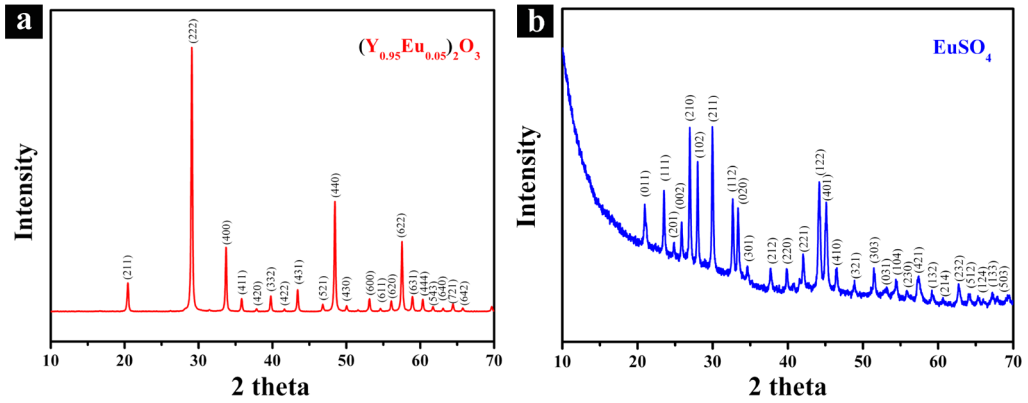

Figure 2. XRD patterns of (a) the as-obtained Y_2O_3/Eu_2O_3 mixtures and (b) recycled $EuSO_4$.

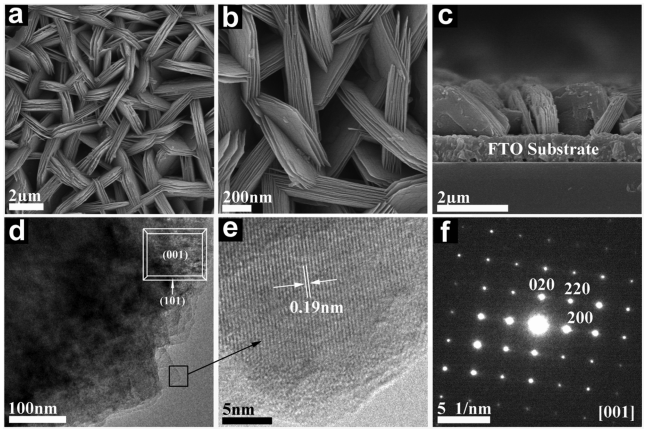

Figure 3. SEM images of anatase Y-doped TiO_2 nanosheets film with exposed {001} facets on FTO substrate synthesized by a solvothermal approach at 200 °C for 12 h: (a) and (b) are top views, and (c) shows a cross-sectional view; (d) TEM image of a detached anatase Y-doped TiO_2 nanosheets film; (e) HR-TEM image recorded from the TiO_2 nanosheets side surface marked with a rectangle and (f) the corresponding SAED patterns recorded from (e).

the sample (Figure 3b) displays that the TiO_2 nanosheets have a highly ordered arrangement with well-defined layer-by-layer structures, and the thickness of an individual nanosheets was approximately 20 nm. A cross-sectional view of the Y-doped TiO_2 nanosheets film in Figure 3c shows that the film thickness is approximately 1.3 μm. Figure 3c also confirms that these nanosheets are composed of layer-by-layer structures.

Well-defined sheet-shaped TiO_2 structures are clearly observable in the TEM image in Figure 3d. Figure 3e shows a high-resolution TEM image recorded from Figure 3d, which evidently showed that the lattice spacing parallel to the top and bottom facets was 0.19 nm, agreeing well with the spacing of the (200) and (020) lattice planes of anatase type TiO_2.[24,25] The same region of SAED patterns (Figure 3f) can be indexed into the diffraction spots of the [001] zone, indicating that the top and bottom surfaces of the TiO_2 nanosheets are high-energy {001} facets. The clear diffraction spots also indicate the single crystalline nature of the nanosheets (Figure 3f). These structural analyses indicate that the prepared Y-doped TiO_2 nanosheets are dominated by the {001} facets, and the corresponding percentage of exposed {001} facets is statistically estimated to be 97%. Energy dispersive analysis of X-rays (EDAX) analysis result confirms the presence of Y in the TiO_2 nanosheets film and the doping concentration of Y is low at approximately 0.3 wt % (Figure S3). These results confirmed that the Y-doped TiO_2 nanosheets film with dominant {001} facets was successfully synthesized by the proposed solvothermal method.

The typical XRD pattern of the as-synthesized Y-doped TiO_2 nanosheets film was measured (Figure 4). As depicted in Figure 4a, the as-synthesized sample showed peaks at 2θ values of 25.3°, 36.9°, 37.8°, 38.5°, 48.1°, 53.9°, 55.1°, 62.1°, and 62.7°, corresponding to the anatase (101), (103), (004), (112), (200), (105), (211), (213), and (204) crystal planes (JCPDS No. 21-1272), respectively. In addition, the peak of the (100) crystalline phase of hexagonal $TiOF_2$ (JCPDS No. 77-0132) was visible. After calcination at 600 °C for 2 h, the as-synthesized sample transformed into pure anatase TiO_2 phase with high crystallization (Figure 4b). The diffraction peaks of $TiOF_2$ completely disappeared, indicating that F ions in $TiOF_2$ are easily removed by the annealing treatment. No crystalline phase for the yttrium oxides was observed. This absence can possibly be attributed to the very small level as determined from the EDAX results and uniform dispersion of Y^{3+} ions in the TiO_2 nanocrystals, similar to reported behavior for La doping.[26,27]

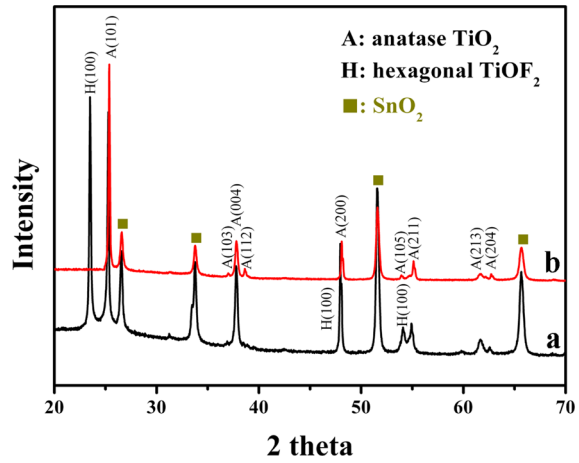

Figure 4. XRD patterns of Y-doped TiO_2 nanosheets film: (a) as-synthesized by solvothermal treatment at 200 °C for 12 h; (b) after annealing at 600 °C for 2 h.

The DRS spectra were used to evaluate the light absorption and band gap of as-prepared Y-doped TiO_2 samples, as shown in Figure S4. It can be clearly seen that a slight shift of the absorption profile was observed for Y-doped TiO_2 nanosheets,

DOI: 10.1021/acssuschemeng.5b01783
ACS Sustainable Chem. Eng. 2016, 4, 1794−1803

compared with pure P25 TiO_2 (Figure S4a). For further study of the change gap of Y-doped TiO_2 nanosheets, the plots of $[F(R-E)]^{1/2}$ *vs.* photon energy is shown in Figure S4b. It can be found that the band gap of TiO_2 was narrowed from 3.25 to 3.04 eV after Y-doped. The results show that the Y^{3+} ions doping reduced the band gap of TiO_2.

To confirm the surface composition and chemical states of the elements, the as-prepared anatase Y-doped TiO_2 nanosheets film were investigated by XPS (Figure 5). The O 1s

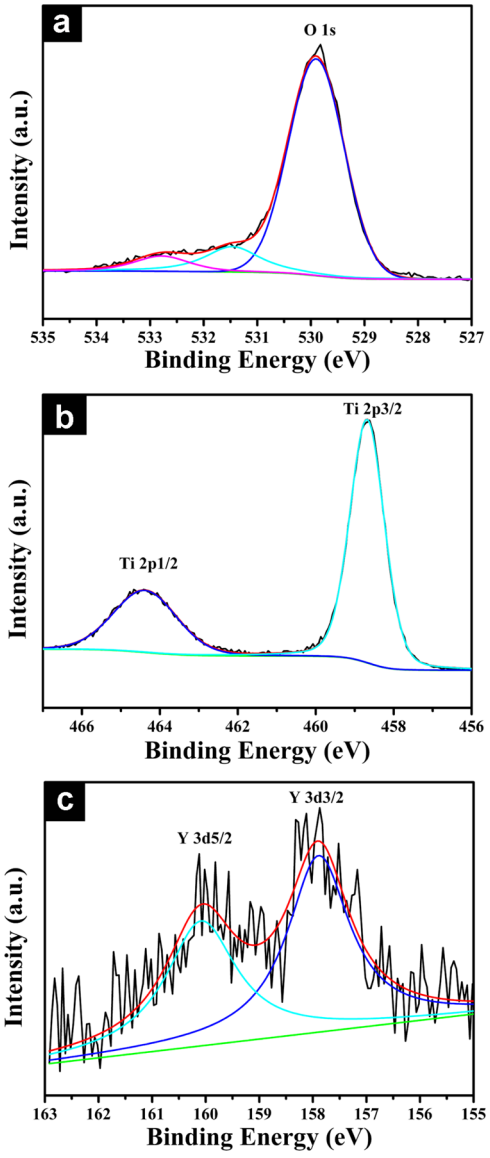

Figure 5. High-resolution XPS spectra of the as-prepared Y-doped TiO_2 nanosheets sample for (a) O 1s, (b) Ti 2p, and (c) Y 3d peaks.

peaks appearing at 529.9 and 531.5 eV were attributed to the lattice oxygen and the hydroxyl groups, respectively (Figure 5a).[28] It has been reported that the hydroxyl groups can react with photoinduced holes to yield highly oxidizing surface-bound ·OH radicals.[29] Additionally, the O 1s spectrum exhibited a third peak at approximately 532.8 eV corresponding to the Y−O bonds. The binding energies of Ti $2p_{3/2}$ and Ti $2p_{1/2}$ are approximately 458.7 and 464.5 eV (Figure 5b), respectively.[2] The splitting difference of 5.8 eV between the two bands indicates that Ti was present as Ti^{4+} in the sample. The two peaks of the Ti 2p energy levels in Y-doped TiO_2 nanosheets film are slightly shifted toward higher energies compared with the valves of pure TiO_2 (Figure S5), implying that the yttrium ions may be incorporated into the TiO_2 lattice. The Y $3d_{3/2}$ and Y $3d_{5/2}$ peaks with binding energies at 160.1 and 157.9 eV, respectively, are in agreement with the Y−OH bond reported in the literature (Figure 5c).[30]

To study the growth mechanism of the Y-doped TiO_2 nanosheets film with dominated highly reactive {001} facets, samples with different reaction times were investigated. Figure 6a−e shows typical SEM images of the as-synthesized Y-doped TiO_2 nanosheets film under different reaction times. It shows that only a thin layer of TiO_2 spherical nanoparticles and octahedral nanorods can be obtained on the FTO substrate with 1 h of crystallization (Figure 6a). With 3 h of growth time, sparse sheet-shaped TiO_2 structures were formed with a thickness of approximately 350 nm (Figure 6b). When the growth time was increased to 6 h, the sheet-shaped TiO_2 filled the FTO substrate, and the average thickness increased to 1.3 μm (Figure 6c). The higher magnification SEM image shown in the lower row in Figure 6c reveals that the sheet-shaped TiO_2 were eroded by exfoliation into a layer-by-layer nanosheets structure that appeared on the central parts of the plane crystal facets. This observed erosion by exfoliation phenomena may be due to HF etching or dissolution effect on TiO_2 {001} facets.[31] Further erosion by exfoliation on the sheet-shaped crystal facets was observed, and the thickness of the sheet-shaped structure was decreased to approximately 600 nm after 9 h of reaction (Figure 6d). After 12 h of growth, the sheet-shaped TiO_2 was completely eroded/exfoliated and replaced by irregular-shaped layer-by-layer nanosheets structure (Figure 6e). Moreover, the thickness of an individual nanosheet was also decreased to approximately 20 nm as shown in the higher magnification SEM image (lower row) in Figure 6e.

On the basis of the experimental results, a proposed growth mechanism of the Y-doped TiO_2 nanosheets film with dominant {001} facets is given in Figure 6f. Initially, $Ti(OBu)_4$ reacted with acetic acid and formed TiO_2 nanoparticles according to the following reaction (eqs 1 and 2):[32,33]

$$\equiv Ti-O-C_4H_9 + CH_3COOH \rightarrow \equiv Ti-OH + CH_3COOC_4H_9 \quad (1)$$

$$\equiv Ti-OH + HO-Ti\equiv \rightarrow \equiv Ti-O-Ti\equiv + H_2O \quad (2)$$

Then, these primary nanoparticles continuously grew along the [001] direction to form TiO_2 nanosheets in the presence of fluoride ions. However, it has been reported that TiO_2 {001} facets synthesized at a high HF concentration can also be seriously eroded by HF (eq 3):[31]

$$-TiOF_2 + 2HF \xrightarrow{\text{dissolution}} TiF_4\cdots H_2O \quad (3)$$

Thus, in the continuing reaction, the crystal growth is slower than the HF etching/dissolution, the TiO_2 {001} facets are eroded by exfoliation, and the thickness of the nanosheets decreases to form layer-by-layer nanosheets structures.

Evaluation of Photocatalytic Activities. Dye effluents from textile industries are becoming a serious environmental problem, as they are stable in light and resistant to chemical and biological degradation. In addition, hexavalent chromium (Cr(VI)) contamination in groundwater is a global environmental problem that poses a health risk to humans because of its high acute toxicity and carcinogenic activity. Photocatalysis

DOI: 10.1021/acssuschemeng.5b01783
ACS Sustainable Chem. Eng. 2016, 4, 1794−1803

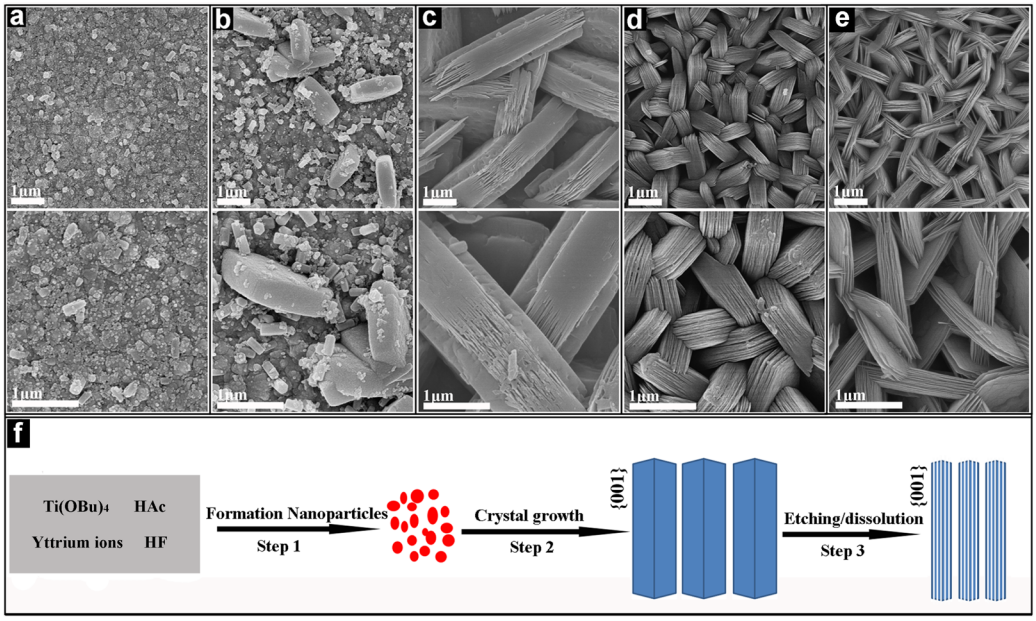

Figure 6. SEM images of Y-doped TiO_2 nanosheets film obtained at different reaction times: (a) 1 h, (b) 3 h, (c) 6 h, (d) 9 h, and (e) 12 h. (f) Schematic illustration of the possible growth mechanism of Y-doped TiO_2 nanosheets film.

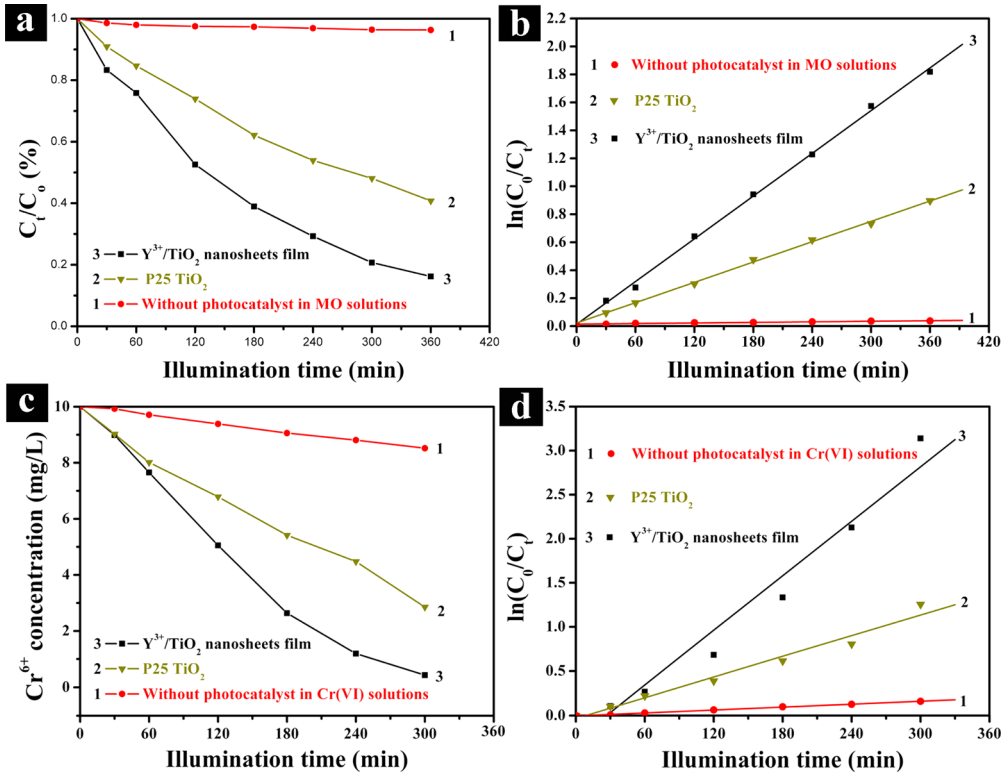

Figure 7. Photocatalytic degradation of (a) MO and (c) Cr(VI) in the presence and absence of the photocatalysts under UV light irradiation; photocatalytic reaction kinetics of (b) MO and (d) Cr(VI) with reaction time.

in the presence of nanostructured TiO_2 has been proven to be effective for the removal of various harmful pollutants.[3] Therefore, the photocatalytic efficiency of MO and Cr(VI) was evaluated using the as-prepared Y-doped TiO_2 nanosheets film under the UV irradiation of a 30 W high-pressure Hg lamp. For comparison purpose, the photocatalytic oxidation of MO and reduction of Cr(VI) by P25 TiO_2 (a benchmark photocatalyst for photocatalytic activity evaluation) was also conducted, as shown in Figure 7.

Figure 7a,c shows the photocatalytic oxidation of MO and the reduction of Cr(VI) under UV light irradiation in the presence and absence of the photocatalysts, respective. Blank experiments suggested that the concentration changes of MO and Cr(VI) under UV light irradiation without the photocatalyst could be ignored (curve 1 in Figure 7a,c). Significantly,

DOI: 10.1021/acssuschemeng.5b01783
ACS Sustainable Chem. Eng. 2016, 4, 1794−1803

the Y-doped TiO_2 nanosheets film with dominant {001} facets (curve 3 in Figure 7a,c) exhibit a higher photocatalytic activity than P25 TiO_2 (curve 2 in Figure 7a,c) both in the MO system or the Cr(VI) system. For example, after UV irradiation for 360 min, 82.8% of MO is photodegraded on the Y-doped TiO_2 nanosheets film, compared with a 59.3% reduction by P25 TiO_2. And after 300 min of UV light irradiation, the Cr(VI) removal was 96%, compared with a 71.5% reduction by P25 TiO_2.

The absorption spectrum of MO in the presence of the Y-doped TiO_2 nanosheets film under exposure to UV light for various durations in the photocatalytic degradation process was also shown in Figure S6. It can be seen that the absorption peak at η = 464 nm diminishes gradually as the exposure time increases and no new absorption bands appear in either the visible light or the UV region. This indicates the complete degradation of MO by photocatalyzed reactions.

To compare quantitatively the photocatalytic activities, the apparent rate constant (κ_{app}) for photocatalytic oxidation of MO and reduction of Cr(VI) over the film samples was evaluated using a pseudo-first-order model (eq 4),[34] as shown in Figure 7b,d:

$$\ln(C_0/C_t) = \kappa_{app} t \quad (4)$$

where κ_{app} is the apparent rate constant, C_t is the solution-phase concentration of dye, and C_0 is the initial concentration at $t = 0$. The apparent rate constant κ_{app} values are also listed in Table 2.

Table 2. Reaction Constant κ_{app} (min^{-1}) in the MO and Cr(VI) with Various TiO_2 Samples

samples	decontamination of MO	decontamination of Cr(VI)
Y-doped TiO_2 nanosheets	5.11×10^{-3} min^{-1}	1.03×10^{-2} min^{-1}
P25 TiO_2	2.45×10^{-3} min^{-1}	3.89×10^{-3} min^{-1}

In the MO system, the Y-doped TiO_2 nanosheets film with dominant {001} facets show the higher photocatalytic activity with a rate constant of 5.11×10^{-3} min^{-1}, which is larger than that of P25 TiO_2 (2.45×10^{-3} min^{-1}) by a factor of 2.09. In the Cr(VI) system, the calculate rate constant for P25 TiO_2 is 3.89×10^{-3} min^{-1}. In strong contrast, the rate constant of 1.03×10^{-2} min^{-1} is obtained from Y-doped TiO_2 nanosheets film, almost three times larger than that of P25 TiO_2.

The photocatalytic oxidation of MO and reduction of Cr(VI) was cycled 7 times under the same conditions used to investigate the stability of the Y-doped TiO_2 nanosheets film, as shown in Figure S7. No obviously deactivation was observed in the cycling tests for the photoreduction of MO and Cr(VI) on the Y-doped TiO_2 nanosheets film, indicating that it possesses outstanding photocatalytic stability.

Proposed Mechanism. The possible mechanism is proposed in Figure 8, which shows the possible reactions in the photocatalysis process. Figure 8a shows the proposed reactions in the photocatalytic oxidation of MO on the Y-doped TiO_2 nanosheets under UV light irradiation. The whole reaction mechanism starts with the electron–hole pair created in TiO_2 under UV light irradiation (eq 5).

$$TiO_2 + h\nu \rightarrow h^+ + e^- \quad (5)$$

The separation efficiency of photogenerated electron–hole pairs determines photocatalytic properties. It has been known

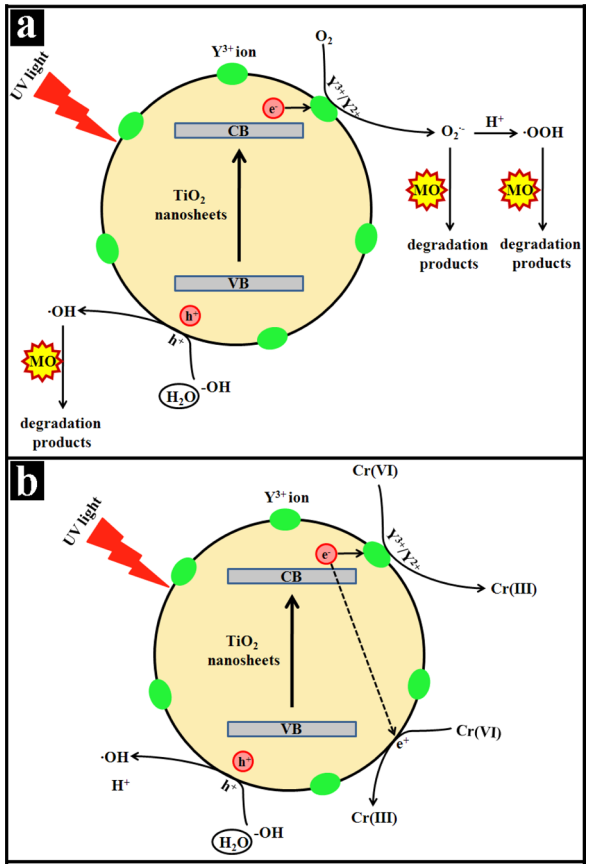

Figure 8. Schematic diagram of a possible mechanism of (a) photocatalytic oxidation of MO and (b) photocatalytic reduction of Cr(VI) on the Y-doped TiO_2 nanosheets under UV light irradiation.

that TiO_2 modification with lanthanides ions yield excellent electrons scavenging capacity.[34,35] Thus, we used the PL technique to define the separation capacity of photogenerated electrons and holes. Figure S8 illustrates the room-temperature PL spectra of the as-obtained Y-doped TiO_2 and pure P25 TiO_2 samples under the excitation wavelength of 355 nm. Compared with the pure P25 TiO_2, the Y-doped TiO_2 samples obviously exhibit lower intensity of emission spectrum, which clearly indicates that a more efficient transfer and separation of photogenerated electrons and holes caused by doped Y^{3+} ions. Therefore, the photogenerated electrons are quickly trapped by the Y^{3+} ions in Y-doped TiO_2 system (eq 6), resulting in the formation of Y^{2+}.[36] The unstable Y^{2+} ions may also react with adsorbed O_2, thus forming highly reactive superoxide ions ($O_2^{\cdot-}$) (eq 7).

$$Y^{3+} + e^- \rightarrow Y^{2+} \quad (6)$$

$$Y^{2+} + O_2 \rightarrow Y^{3+} + O_2^{\cdot-} \quad (7)$$

Through a series of redox reactions, a number of charged species and radicals with high redox potentials are generated (eqs 8–10).

$$O_2^{\cdot-} + H^+ \rightarrow \cdot OOH \quad (8)$$

$$2\cdot OOH \rightarrow O_2 + H_2O_2 \quad (9)$$

$$H_2O_2 + e^- \rightarrow \cdot OH \quad (10)$$

DOI: 10.1021/acssuschemeng.5b01783
ACS Sustainable Chem. Eng. 2016, 4, 1794–1803

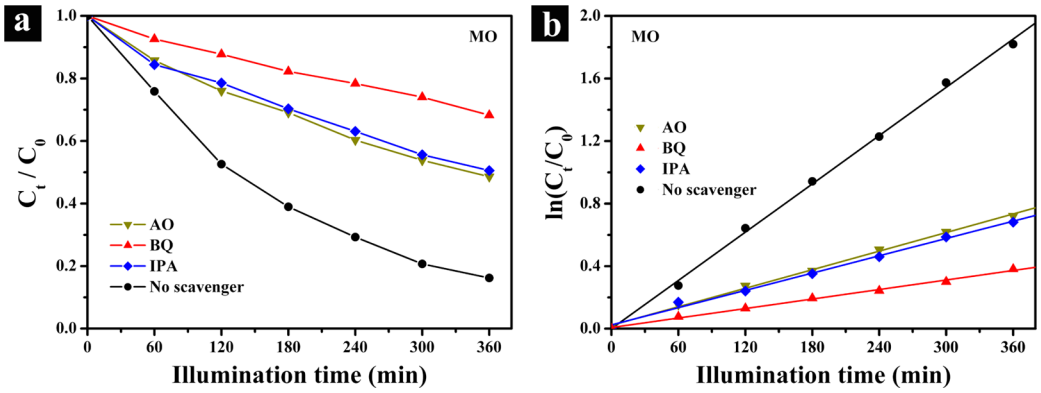

Figure 9. Effects of different scavengers on the MO photodegradation process under UV light irradiation: (a) photodegradation efficiency, and (b) photocatalytic reaction kinetics.

In addition, it has been widely reported that surface O molecules on the {001} facets are unstable and very reactive, which leads to more oxygen vacancies on the exposed {001} facets.[37] The defects caused by these oxygen vacancies can provide sites for the photogenerated holes to react with dissociated water molecules and hydroxyl groups, thus forming ·OH radicals (eqs 11 and 12):

$$h^+ + H_2O \rightarrow \cdot OH + H^+ \quad (11)$$

$$h^+ + (-OH) \rightarrow \cdot OH \quad (12)$$

As a result, these highly oxidizing species can be strongly reactive with organic molecules to produce degradation products (eqs 13 and 14).

$$O_2^{\cdot -} + MO \rightarrow \text{degradation of products} \quad (13)$$

$$\cdot OH + MO \rightarrow \text{degradation of products} \quad (14)$$

Figure 8b shows the possible reactions in the photocatalytic reduction of Cr(VI) on the Y-doped TiO_2 nanosheets under UV light irradiation. For the removal of Cr(VI) in the reaction systems, first, TiO_2 nanosheets were excited to generate electron–hole pairs (eq 5). Then, the photogenerated electrons can directly reduce adsorbed Cr(VI) to Cr(III) according to eq 15.[38] In the Y-doped TiO_2 nanosheets, the Y^{3+} ions are reduced to Y^{2+} by the photoelectrons from TiO_2 nanosheets according to eq 6.[36] Then, the unstable Y^{2+} ions can easily reduce Cr(VI) to Cr(III) according to eq 16. Adsorbed H_2O or hydroxyl groups accepted holes in eqs 7 and 8), thus forming ·OH radicals, and the photocatalysis redox cycle thereby continued, resulting in an enhanced Cr(VI) removal capacity in the Y-doped TiO_2 nanosheets.

$$3e^- + Cr(VI) \rightarrow Cr(III) \quad (15)$$

$$3Y^{2+} + Cr(VI) \rightarrow 3Y^{3+} + Cr(III) \quad (16)$$

With the purpose of understanding the role of the those active species during the photodegradation of MO over Y-doped TiO_2 nanosheets film, ammonium oxalate (AO, 1 mM), benzoquinone (BQ, 1 mM) and isopropyl alcohol (IPA, 1 mM) were used as scavenging reagents for h^+, $O_2^{\cdot -}$, and ·OH, respectively.[39,40] Figure 9a,b displays the photocatalytic activities of MO over Y-doped TiO_2 nanosheets film under different scavengers. The addition of BQ can reduce the photocatalytic efficiency of MO to the largest extent, indicating that $O_2^{\cdot -}$ can be generated by photoelectrons reacting with adsorbed O_2 and served as the main active species during the photodegradation process. When added IPA and AO into the MO system, the photocatalytic activities of MO decreased to some degree, suggesting that the h^+ and ·OH radicals contribute almost equally and moderately during the photodegradation process. However, the results also show that the h^+ contribute a less extent than ·OH radicals. Thus, it can be concluded that the reaction (eqs 8–10) may occur to generate more ·OH radicals during the photocatalytic process.

CONCLUSIONS

In summary, CRT waste is right with yttrium oxide and europium oxide, which makes this waste useful for recovering high-value REEs. Moreover, these recycled REEs are useful to prepare low-cost sustainable photocatalytic materials. In this work, we have successfully prepared Y-doped anatase TiO_2 nanosheets film with exposed {001} facets using cheap recycled yttrium as a dopant source, which was derived from CRT phosphor waste. The as-prepared Y-doped TiO_2 nanosheets film exhibit a layer-by-layer self-assembled structure. Observation by TEM and SEM confirmed the TiO_2 nanosheets with dominant {001} facets, and the percentage of these facets was statistically estimated to be 97%. The presence of the element Y in TiO_2 nanosheets film was verified by EDAX and XPS analyses. A possible growth mechanism was postulated by systematically investigating the influence of the reaction time. The formation of layer-by-layer TiO_2 nanosheets structure could be due to an etching/dissolution process under a high HF concentration. Remarkably, the Y-doped TiO_2 nanosheets film exhibit higher photocatalytic efficiency compared with P25 TiO_2 for both oxidation of MO and reduction of Cr(VI). The remarkably improved photocatalytic activity of the Y-doped TiO_2 nanosheets film may be due to the synergistic effect of the efficient separation and transfer of the photogenerated e^-/h^+ pairs due to the presence of the Y^{3+}/Y^{2+} redox couple and the high percentage of exposed {001} facets. Furthermore, Y-doped TiO_2 nanosheets film possesses outstanding photocatalytic stability, showing great potential in the detoxification of harmful pollutants in wastewaters. We hope that this work will not only enrich the recycling methods of CRT phosphor waste but also provide a new means to prepare low-cost sustainable photocatalytic materials using economically viable waste with promising applications in both energy and environmental fields.

DOI: 10.1021/acssuschemeng.5b01783
ACS Sustainable Chem. Eng. 2016, 4, 1794–1803

■ ASSOCIATED CONTENT

Supporting Information

The Supporting Information is available free of charge on the ACS Publications website at DOI: 10.1021/acssuschemeng.5b01783.

The experiment photograph, the SEM, XRD, EDX, XPS, DRS, and PL results of the sample, the photocatalytic stability of the sample, and chemical compositions results (PDF).

■ AUTHOR INFORMATION

Corresponding Authors

*Q. Zhang. Fax: +86-10-67396234. Tel: +86-10-67396234. E-mail: zhangqijun@bjut.edu.cn.

*Y. Wu. Fax: +86-10-67396234. Tel: +86-10-67396234. E-mail: wuyufeng@bjut.edu.cn.

Notes

The authors declare no competing financial interest.

■ ACKNOWLEDGMENTS

This research was financially supported by Beijing Nova Program (Z1511000003150141), National Natural Scientic Foundation of China (No. 21306004), Academician Workstation in Yunnan Province, and Key Discipline for Resource, Environment & Circular Economy of Beijing.

■ REFERENCES

(1) Zhang, H.; Liu, P.; Li, F.; Liu, H.; Wang, Y.; Zhang, S.; Guo, M.; Cheng, H.; Zhao, H. Facile fabrication of anatase TiO_2 microspheres on solid substrates and surface crystal facet transformation from {001} to {101}. *Chem. - Eur. J.* **2011**, *17*, 5949−5957.

(2) Zhang, Q.; Sun, C.; Zhao, Y.; Zhou, S.; Hu, X.; Chen, P. Low Ag-doped titanium dioxide nanosheet film with outstanding antimicrobial property. *Environ. Sci. Technol.* **2010**, *44*, 8270−8275.

(3) Altin, I.; Sökmen, M. Preparation of TiO_2-polystyrene photocatalyst from waste material and its usability for removal of various pollutants. *Appl. Catal., B: Environ.* **2014**, *144*, 694−701.

(4) Quesada-Cabrera, R.; Sotelo-Vazquez, C.; Darr, J. A.; Parkin, I. P. Influence of surface nitrogen species on the activity of N-doped TiO_2 thin-film during photodegradation of stearic acid under UV light irradiation. *Appl. Catal., B: Environ.* **2014**, *160−161*, 582−588.

(5) Wu, Q.; Zhao, J.; Qin, G.; Wang, C.; Tong, X.; Xue, S. Photocatalytic reduction of Cr(VI) with TiO_2 film under visible light. *Appl. Catal., B: Environ.* **2013**, *142−143*, 142−148.

(6) Liu, B.; Aydil, E. S. Anatase TiO_2 film with reactive {001} facets on transparent conductive substrate. *Chem. Commun.* **2011**, *47*, 9507−9509.

(7) Zhang, M.; Yuan, S.; Wang, Z. Y.; Shi, L. Photoelectrocatalytic properties of Cu^{2+}-doped TiO_2 film under visible light. *Appl. Catal., B: Environ.* **2013**, *134−135*, 185−192.

(8) Yao, Z.; Jia, F.; Tian, S.; Li, C.; Jiang, Z.; Bai, X. Microporous Ni-doped TiO_2 film photocatalyst by plasma electrolytic oxidation. *ACS Appl. Mater. Interfaces* **2010**, *2*, 2617−2622.

(9) Lee, W. J.; Lee, J. M.; Kochuveedu, S. T.; Han, T. H.; Jeong, H. Y.; Park, M.; Yun, J. M.; Kwon, J.; No, K.; Kim, D. H.; Kim, S. O. Biomineralized N-doped CNT/TiO_2 core/shell nanowires for visible light photocatalysis. *ACS Nano* **2012**, *6*, 935−943.

(10) Bingham, S.; Daoud, W. A. Recent advances in making nano-sized TiO_2 visible-light active through rare-earth metal doping. *J. Mater. Chem.* **2011**, *21*, 2041−2050.

(11) Zhang, W.; Wang, K.; Zhu, S.; Li, Y.; Wang, F.; He, H. Yttrium-doped TiO_2 film prepared by means of DC reactive magnetron sputtering. *Chem. Eng. J.* **2009**, *155*, 83−87.

(12) Chen, M.; Zhang, F. S.; Zhu, J. Lead recovery and the feasibility of foam glass production from funnel glass of dismantled cathode ray tube through pyrovacuum process. *J. Hazard. Mater.* **2009**, *161*, 1109−1113.

(13) Xu, Q.; Li, G.; He, W.; Huang, J.; Shi, X. Cathode ray tube (CRT) recycling: Current capabilities in China and research progress. *Waste Manage.* **2012**, *32*, 1566−1574.

(14) Innocenzi, V.; De Michelis, I.; Ferella, F.; Beolchini, F.; Kopacek, B.; Vegliò, F. Recovery of yttrium from fluorescent powder of cathode ray tube, CRT: Zn removal by sulphide precipitation. *Waste Manage.* **2013**, *33*, 2364−2371.

(15) Andreola, F.; Barbieri, L.; Corradi, A.; Lancellotti, I. CRT glass state of the art: A case study: Recycling in ceramic glazes. *J. Eur. Ceram. Soc.* **2007**, *27*, 1623−1629.

(16) Lu, X.; Shih, K.; Liu, C.; Wang, F. Extraction of metallic lead from cathode ray tube (CRT) funnel glass by thermal reduction with metallic iron. *Environ. Sci. Technol.* **2013**, *47*, 9972−9978.

(17) Yang, H.; Sun, C.; Qiao, S.; Zou, J.; Liu, G.; Smith, S. C.; Cheng, H.; Lu, G. Anatase TiO_2 single crystals with a large percentage of reactive Facets. *Nature* **2008**, *453*, 638−641.

(18) Wang, J.; Bian, Z.; Zhu, J.; Li, H. Ordered mesoporous TiO_2 with exposed (001) facets and enhanced activity in photocatalytic selective oxidation of alcohols. *J. Mater. Chem. A* **2013**, *1*, 1296−1302.

(19) Han, X.; Kuang, Q.; Jin, M.; Xie, Z.; Zheng, L. Synthesis of titania nanosheets with a high percentage of exposed (001) facets and related photocatalytic properties. *J. Am. Chem. Soc.* **2009**, *131*, 3152−3153.

(20) Liu, M.; Piao, L.; Lu, W.; Ju, S.; Zhao, L.; Zhou, C.; Li, H.; Wang, W. Flower-like TiO_2 nanostructures with exposed {001} facets: Facile synthesis and enhanced photocatalysis. *Nanoscale* **2010**, *2*, 1115−1117.

(21) Liu, S.; Yu, J.; Cheng, B.; Jaroniec, M. Fluorinated semiconductor photocatalysts: tunable synthesis and unique properties. *Adv. Colloid Interface Sci.* **2012**, *173*, 35−53.

(22) Van den Bogaert, B.; Havaux, D.; Binnemans, K.; Van Gerven, T. Photochemical recycling of europium from Eu/Y mixtures in red lamp phosphor waste streams. *Green Chem.* **2015**, *17*, 2180−2187.

(23) Ito, S.; Chen, P.; Comte, P.; Nazeeruddin, M. K.; Liska, P.; Pechy, P. Fabrication of screen printing pastes from TiO_2 powders for dye-sensitised solar cells. *Prog. Photovoltaics* **2007**, *15*, 603−612.

(24) Chen, J. S.; Tan, Y. L.; Li, C. M.; Cheah, Y. L.; Luan, D. Y.; Madhavi, S.; Boey, F. Y. C.; Archer, L. A.; Lou, X. W. Constructing hierarchical spheres from large ultrathin anatase TiO_2 nanosheets with nearly 100% exposed (001) facets for fast reversible lithium storage. *J. Am. Chem. Soc.* **2010**, *132*, 6124−6130.

(25) Sun, L.; Zhai, J.; Li, H.; Zhao, Y.; Yang, H.; Yu, H. Study of homologous elements: Fe, Co, and Ni dopant effects on the photoreactivity of TiO_2 nanosheets. *ChemCatChem* **2014**, *6*, 339−347.

(26) Chandiran, A. K.; Sauvage, F.; Etgar, L.; Graetzel, M. Ga^{3+} and Y^{3+} cationic substitution in mesoporous TiO_2 photoanodes for photovoltaic applications. *J. Phys. Chem. C* **2011**, *115*, 9232−9240.

(27) Long, L.; Zhang, A.; Yang, J.; Zhang, X.; Yu, H. A green approach for preparing doped TiO_2 single crystals. *ACS Appl. Mater. Interfaces* **2014**, *6*, 16712−16720.

(28) Pan, J. H.; Lee, W. I. Preparation of highly ordered cubic mesoporous WO_3/TiO_2 film and their photocatalytic properties. *Chem. Mater.* **2006**, *18*, 847−853.

(29) He, Z.; Que, W.; Chen, J.; Yin, X.; He, Y.; Ren, J. Photocatalytic degradation of methyl orange over nitrogen-fluorine codoped TiO_2 nanobelts prepared by solvothermal synthesis. *ACS Appl. Mater. Interfaces* **2012**, *4*, 6816−6826.

(30) Mongstad, T.; Thøgersen, A.; Subrahmanyam, A.; Karazhanov, S. The electronic state of thin film of yttrium, yttrium hydrides and yttrium oxide. *Sol. Energy Mater. Sol. Cells* **2014**, *128*, 270−274.

(31) Wang, Y.; Zhang, H.; Han, Y.; Liu, P.; Yao, X.; Zhao, H. A selective etching phenomenon on {001} faceted anatase titanium dioxide single crystal surfaces by hydrofluoric acid. *Chem. Commun.* **2011**, *47*, 2829−2831.

(32) Zhang, Z.; Zhong, X.; Liu, S.; Li, D.; Han, M. Aminolysis route to monodisperse titania nanorods with tunable aspect ratio. *Angew. Chem., Int. Ed.* **2005**, *44*, 3466−3470.

(33) Liu, Y.; Liu, R.; Liu, C.; Luo, S.; Yang, L.; Sui, F.; Teng, Y.; Yang, R.; Cai, Q. Enhanced photocatalysis on TiO_2 nanotube arrays modified with molecularly imprinted TiO_2 thin film. *J. Hazard. Mater.* **2010**, *182*, 912−918.
(34) Reszczyńska, J.; Grzyb, T.; Sobczak, J. W.; Lisowski, W.; Gazda, M.; Ohtani, B.; Zaleska, A. Visible light activity of rare earth metal doped (Er^{3+}, Yb^{3+} or Er^{3+}/Yb^{3+}) titania photocatalysts. *Appl. Catal., B: Environ.* **2015**, *163*, 40−49.
(35) Reszczyńska, J.; Grzyb, T.; Wei, Z.; Klein, M.; Kowalska, E.; Ohtani, B. A. Photocatalytic activity and luminescence properties of RE^{3+}-TiO_2 nanocrystals prepared by sol-gel and hydrothermal methods. *Appl. Catal., B: Environ.* **2016**, *181*, 825−837.
(36) Ökte, A. N.; Yılmaz, Ö. Photodecolorization of methyl orange by yttrium incorporated TiO_2 supported ZSM-5. *Appl. Catal., B: Environ.* **2008**, *85*, 92−102.
(37) Yu, L.; Yang, X.; He, J.; He, Y.; Wang, D. A fluorine free method to synthesize nitrogen and lanthanum co-doped TiO_2 nanocrystals with exposed {001} facets for enhancing visible-light photocatalytic activity. *J. Mol. Catal. A: Chem.* **2015**, *399*, 42−47.
(38) Lu, D.; Fang, P.; Liu, X.; Zhai, S.; Li, C.; Zhao, X.; Ding, J.; Xiong, R. A facile one-pot synthesis of TiO_2-based nanosheets loaded with Mn_xO_y nanoparticles with enhanced visible light-driven photocatalytic performance for removal of Cr(VI) or RhB. *Appl. Catal., B: Environ.* **2015**, *179*, 558−573.
(39) Tan, C.; Zhu, G.; Hojamberdiev, M.; Lokesh, K. S.; Luo, X.; Jin, L.; Zhou, J.; Liu, P. Adsorption and enhanced photocatalytic activity of the {0001} faceted Sm-doped $ZnIn_2S_4$ microspheres. *J. Hazard. Mater.* **2014**, *278*, 572−583.
(40) Luo, X.; Zhu, G.; Peng, J.; Wei, X.; Hojamberdiev, M.; Jin, L.; Liu, P. Enhanced photocatalytic activity of Gd-doped porous β-Bi_2O_3 photocatalysts under visible light irradiation. *Appl. Surf. Sci.* **2015**, *351*, 260−269.

DOI: 10.1021/acssuschemeng.5b01783
ACS Sustainable Chem. Eng. 2016, 4, 1794−1803